www.czasopisma.pan.pl PAN www.journals.pan.pl
POLSKA AKADEMIA NAUK

Metrol. Meas. Syst., Vol. 24 (2017), No. 2, pp. 413–424.

PAN POLSKA AKADEMIA NAUK

METROLOGY AND MEASUREMENT SYSTEMS

Index 330930, ISSN 0860-8229

www.metrology.pg.gda.pl

M&MS

MODELLING OF MECHANICAL BEHAVIOUR OF HIGH-FREQUENCY PIEZOELECTRIC ACTUATORS USING BOUC-WEN MODEL

Rafał Kędra, Magdalena Rucka

Gdańsk University of Technology, Faculty of Civil and Environmental Engineering, G. Narutowicza 11/12, 80-233 Gdańsk, Poland (rafkedra@pg.gda.pl, ✉ mrucka@pg.gda.pl, +48 58 347 2497*)*

Abstract

The paper presents application of a modified, symmetrical Bouc-Wen model to simulate the mechanical behaviour of high-frequency *piezoelectric actuators* (PAs). In order to identify parameters of the model, a two-step algorithm was developed. In its first stage, the mechanical parameters were identified by taking into account their bilinear variability and using a square input voltage waveform. In the second step, the hysteresis parameters were determined based on a periodic excitation. Additionally, in order to reduce the influence of measurement errors in determination of selected derivatives the *continuum wavelet transform* (CWT) and *translation-rotation transformation* (TRT) methods were applied. The results proved that the modified symmetrical Bouc-Wen model is able to describe the mechanical behaviour of PAs across a wide frequency range.

Keywords: piezoelectric actuators, Bouc-Wen model, parameters identification.

1. Introduction

High-frequency *piezoelectric actuators* (PAs) are widely used as components of *structural health monitoring* (SHM) and damage detection systems based of the phenomenon of elastic waves' propagation. They can operate in a wide frequency range, varying from 10 kHz to 500 kHz, depending on the properties of a monitored structure and the applied SHM method. The main advantages are their durability, small size and relatively low cost. High-frequency PAs are available in a variety of shapes and configurations and they enable to excite both longitudinal and shear waves. Moreover, using multilayer piezo actuators enables to generate large amplitudes of excitation at a very low operating voltage. This last feature is especially important because increasing the wave amplitude enables to extend the area monitored by an SHM system and to reduce the noise ratio. However, large amplitudes of excitations may result in occurring nonlinearity between the applied voltage and the output displacement, caused by a non-linear relationship between the electric field and strain [1]. This is disadvantageous, since these nonlinearities significantly complicate the damage detection process. Creation of a sensor model accurately describing its nonlinear mechanical behaviour at different voltage and frequency levels can be a solution of this problem. Numerous earlier studies enabled to adapt many mathematical hysteresis models, including the ellipse model [2], the Preisach model [3], the Duhem model [4], the Backlash model [5], the Prandtl-Ishlinskii model [6] and the Bouc-Wen model, to simulate the mechanical behaviour of PAs operating at low and medium frequencies. Especially the Bouc-Wen model has gained in popularity due to its ability to describe various non-linear and hysteretic systems. There are many modifications of this model, which enable to consider the asymmetric hysteresis [7], the frequency-dependent behaviour [8] and the influence of pre-stressing [9]. Combining the rate-dependent Bouc-Wen hysteresis model with a linear dynamic model enabled to model the shape of a displacement-voltage loop in a wide range of frequencies. The experimental tests exhibited a good agreement

Article history: received on Aug. 15, 2016; accepted on Oct. 22, 2016; available online on Jun. 30, 2017; DOI: 10.1515/mms-2017-0022.

of the experimental and numerical results obtained for single [10] and multi-frequency excitations [11]. The research have also indicated that a higher-order dynamic model is required to capture accurately the PA's response for a wide range of excitation frequencies [12]. However, the previous studies have been carried out mainly for the voltage signal frequency not exceeding 1 kHz.

This paper presents the use of a modified symmetrical Bouc-Wen model for simulation of the mechanical behaviour of high-frequency piezoelectric actuators. A two-step algorithm dedicated to parameter identification is developed and experimentally verified on an example of a multilayer piezoelectric plate actuator. The obtained results show that the Bouc-Wen model is able to describe the mechanical behaviour of piezoelectric actuators across a wide frequency range.

2. Bouc-Wen model of hysteresis

The Bouc-Wen model has the ability to describe various non-linear and hysteretic systems. It was formulated by Bouc [13] and extended by Wen [14]. Despite the fact that it does not have an exact analytical solution, the Bouc-Wen model has become a widely used one, due to its comprehensiveness and mathematical tractability. In the case of PAs, besides their conventional formulation, a modified Bouc-Wen model is also used, wherein the hysteresis component is a function of the input voltage. That model can be expressed in a form of two differential equations [15]:

$$m_0 \ddot{x} + c_0 \dot{x} + k_0 (x - x_0) = k_1 u + h, \tag{1}$$

$$\dot{h} = \dot{u}(A - [\beta \operatorname{sgn}(\dot{u} h) + \gamma]|h|^n), \tag{2}$$

where: m_0 – the mass; c_0 – the damping; k_0 – the stiffness; k_1 – the ratio of the input voltage and the driving force; x_0 – the initial displacement; x – a displacement; $\dot{x}$ – the velocity; $\ddot{x}$ – the acceleration; u – the input voltage; h – the restoring (hysteresis) component; and A, β, γ, n – the hysteresis parameters. In a physical sense, the hysteresis component h may be treated as a non-linear component of the voltage-strain relation.

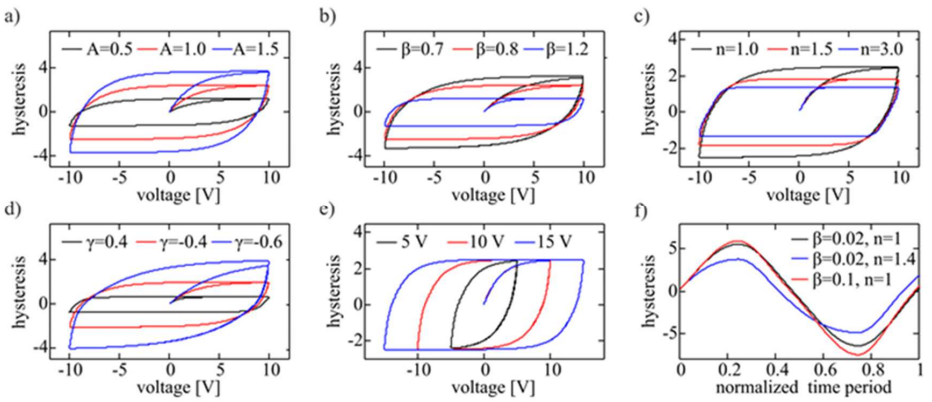

Fig. 1. Variability of the hysteresis component according to (2) for the following parameters: $\beta = 0.8$, $\gamma = -0.4$, $n = 1$(a); $A = 1$, $\gamma = -0.4$, $n = 1$ (b); $A = 1$, $\beta = 0.8$, $\gamma = -0.4$ (c); $A = 1$, $\beta = 0.8$, $n = 1$ (d); $A = 1$, $\beta = 0.8$, $\gamma = -0.4$, $n = 1$ (e); $A = 0.5$, $\gamma = -0.04$ (f).

Metrol. Meas. Syst., Vol. 24 (2017), No. 2, pp. 413–424.

Figures 1a–1d show the influence of individual parameters A, β, γ, n on a change of hysteresis loops for the harmonic input voltage. An increase of the parameter A value causes a proportional increase in the value of hysteresis component h. The opposite effect has a change of the values of parameters β and γ. Moreover, an increase of those parameters reduces the slip effect in the highest voltage area. An increase of the parameter n value leads to reduction of the hysteresis width and, to a smaller extent it is responsible for the smoothing effect. It can be seen that, unlike other parameters, a change of the n value does not lead to a change of the hysteresis component variability in the initial period.

Figure 1e shows the result of a growth of the input voltage amplitude at constant hysteresis parameters. It does not affect the hysteresis amplitude but leads to an extension of the loop. The effect of changing parameter values in the time domain is presented in Fig. 1f. Small values of β and γ result in a similarity of the hysteresis and the input voltage. The effect of the phase shift may be obtained by disproportionate increasing one of them. It should be also noticed that (2) is frequency-independent for a mono-harmonic input voltage.

3. Methodology of parameter identification

Due to a strong nonlinearity of (1) and (2) describing the hysteresis behaviour of PAs, simultaneous identification of all its parameters is possible only by using iterative optimization techniques such as the *particle swarm optimization* (PSO) [16], the *genetic algorithm* (GA) [17] and the *differential evolution* (DE) algorithm [18]. In PSO-based algorithms the initially generated random groups of model and method parameters are called particles. The positions of particles are updated in subsequent steps, taking into account the defined velocity formula. By evaluating the model and calculating the fitness functions, the best location for each particle and the entire group can be determined. Genetic algorithms are based on genetic operations. The response and the fit of a model are evaluated for all initial parameter sets. The best fitting sets are selected to reproduction, crossover and mutation processes resulting in creation of new sets of model parameters. The selection and genetic operations are repeated until the stopping criterion is achieved. DE is similar to GA, the differences lie in the way of carrying out genetic operations. Each new set of parameters is compared with a parent set and the set for which evaluation of the fitness value gives better results is passed to the next iteration. The main problems of iterative approaches are their sensitivity to the initially selected parameters, the possibility of finding only a local minimum, and a relatively slow convergence. Therefore, considering the equations (1) – (2) separately and determining parameters in subsequent steps without iteration is a very convenient alternative [8–9]. This approach significantly reduces the computational cost, simplifies the estimation procedure and enables to avoid ambiguity in determining the parameters related to the occurrence of local minima of optimized functions. It may be used when the hysteresis amplitude is negligible in comparison with the amplitude of the applied input voltage. Such a situation can occur in the case of excitation in a form of a periodic square function and, respectively, a low amplitude. This type of input signal can be defined by an infinite series of sine functions:

$$u_{square} = B\frac{4}{\pi}\sum_{k=1}^{\infty}\frac{\sin(2\pi(2k-1)T_S^{-1}t)}{2k-1}, \tag{3}$$

where B denotes the amplitude and T_S – the period of the square function. In experimental studies the series (3) is limited to a finite number of initial terms. This feature of the excitation signal significantly reduces the hysteresis component value. In the case of PAs operating in a range of frequencies below 1 Hz it is also possible to separate determination of parameters associated with the static hysteresis [7].

3.1. Assessment of mechanical constants

If only the first quarter of the square function period is considered, it can be approximated by the Heaviside step function and used to determine the mechanical parameters using the limit theorem. However, such a simplification does not take into account the time taken by a signal to change from zero to its maximum value (the rise time) and – for the analysed high frequency PAs, where the damping and mass values are much smaller than the stiffness one – it causes large errors. In order to reflect more accurately the variability of the input signal, it can be described as the difference of two time-shifted ramp functions with the same slope:

$$u_1 = a\,t \cdot H(t) - a(t - T_1) \cdot H(t - T_1), \tag{4}$$

where T_1 is the rise time and a – the slope. Assuming that the influence of the hysteresis is neglected ($h << u$) for the input voltage described by (4), the relation (1) after applying the Laplace transform can be written as:

$$m_0 [s^2 X(s) - s\,x(0^-) - \dot{x}(0^-)] + c_0 [s\,X(s) - x(0^-)] + k_0\,X(s) = k_1\,U_1(s), \tag{5}$$

where: $X(s) = \mathcal{L}\left(x(t)\right)$; $U_1(s) = \mathcal{L}\left(u_1(t)\right)$ and $x(0^-)$, $\dot{x}(0^-)$ are the initial displacement and velocity of the PA, respectively. For the zero initial conditions, the relation (5) becomes:

$$X(s) = \frac{k_1}{m_0 s^2 + c_0 s + k_0} U_1(s) = \frac{k_1}{m_0 s^2 + c_0 s + k_0} \frac{a(1 - e^{-T_1 s})}{s^2}. \tag{6}$$

Using the theorem of the limit value, a series of steady-state parameters $K_0, K_1, \ldots, K_n$, can be specified. The first parameter is defined as:

$$K_0 = \lim_{t \to \infty} g_0(t) = \lim_{t \to \infty} x(t) = \lim_{s \to 0} s\,X(s) = \lim_{s \to 0} \frac{k_1\,a(1 - e^{-T_1 s})}{m_0 s^3 + c_0 s^2 + k_0 s} = a T_1 \frac{k_1}{k_0}, \tag{7}$$

and the next ones are described by the following formula:

$$K_i = \lim_{t \to \infty} g_i(t) = \lim_{s \to 0} \frac{1}{s} g_i(s), \tag{8}$$

where g_i is given by the recursive relationship:

$$g_i(t) = \int_0^t [K_{i-1} - g_{i-1}(\tau)] d\tau. \tag{9}$$

Calculation of the limits occurring in the previous formulas for $i = 0, 1, 2, 3$ enables to write the following system of four nonlinear equations with four unknowns: m_0, c_0, k_0 and k_1:

$$\begin{cases} a T_1 \dfrac{k_1}{k_0} = K_0, \\ a T_1^2 \dfrac{k_1}{2 k_0} + K_0 \dfrac{c_0}{k_0} = K_1, \\ a T_1^3 \dfrac{k_1}{6 k_0} + K_1 \dfrac{c_0}{k_0} - K_0 \dfrac{m_0}{k_0} = K_2, \\ a T_1^4 \dfrac{k_1}{24 k_0} + K_2 \dfrac{c_0}{k_0} - K_1 \dfrac{m_0}{k_0} = K_3. \end{cases} \tag{10}$$

Metrol. Meas. Syst., Vol. 24 (2017), No. 2, pp. 413–424.

After multiplying all the equations by the stiffness factor k_0, a linear system of equations with zero values of all free terms will be obtained. This implies that the system (10) is indefinite and it enables to determine a solution only in the case when one of the unknown values is parameterized. In practice, it means that the model does not require determination of all parameters but only their proportions. As a result, (10) can be written in a matrix form using only the first three equations:

$$\begin{bmatrix} K_0 & 0 & 0 \\ K_1 & -K_0 & 0 \\ K_2 & -K_1 & K_0 \end{bmatrix} \begin{bmatrix} k_0 \\ c_0 \\ m_0 \end{bmatrix} = \frac{k_1}{6} \begin{bmatrix} 6aT_1 \\ 3aT_1^2 \\ aT_1^3 \end{bmatrix}. \tag{11}$$

The mechanical parameters of the model are given by:

$$k_0 = aT_1 \mathrm{k}_1 \frac{1}{K_0}, \tag{12}$$

$$c_0 = aT_1 \mathrm{k}_1 \left(\frac{K_1}{K_0^{\,2}} - \frac{T_1}{2K_0} \right), \tag{13}$$

$$m_0 = aT_1 \mathrm{k}_1 \left(\frac{T_1^{\,2}}{6K_0} + \frac{K_1^{\,2} - K_0 K_2}{K_0^{\,3}} - \frac{T_1 K_1}{2K_0^{\,2}} \right). \tag{14}$$

The steady-state parameters K_0, K_1 and K_2 can be determined experimentally using the input voltage in a form of the square function with a sufficiently low amplitude and a long period. The rise time T_1 and the slope a can be determined based on the time variation of input voltage. Finally, the equations (12) to (14) enable to determine the parameters m_0, c_0 and k_0 in relation to the parameter k_1. In order to avoid ambiguity, in the subsequent considerations the arbitrary value of parameter k_1, k_1 = 1 V^{-1} was set.

3.2. Estimation of hysteretic parameters

Based on the known mechanical parameters, for any input voltage u it is possible to reproduce the corresponding hysteresis time variation h. The time derivatives of the hysteresis $\dot{h}$ and input voltage $\dot{u}$ can be also calculated using a simple differential scheme or other techniques of numerical differentiation. The parameters A, β, γ and n appearing in (2) can be estimated using the averaging and the least squares methods. After denoting $z = \dot{h}\,\dot{u}^{-1}$ and $\underline{h} = |h|$, deriving both sides of the (2) gives:

$$\dot{z} = -n[\beta \operatorname{sgn}(\dot{u}\,h) + \gamma]\,\underline{h}^{n-1}\,\dot{\underline{h}}. \tag{15}$$

For time points, where $\dot{u}_i\,h_i > 0$, the above equation can be rewritten in a discrete form:

$$\dot{z}_i = -n(\beta + \gamma)\,\underline{h}_i^{\,n-1}\,\dot{\underline{h}}_i. \tag{16}$$

After taking the logarithms of both sides and doing some mathematical manipulations, (16) can be rewritten as:

$$\ln \frac{\dot{z}_i}{\dot{\underline{h}}_i} = \ln[-n(\beta + \gamma)] + (n-1) \ln \underline{h}_i. \tag{17}$$

Linearization of (17) has been finally made by substituting $q_i = \ln(\dot{z}_i / \dot{\underline{h}}_i)$, $p_i = \ln \underline{h}_i$ and $\nu = \ln[-n(\beta+\gamma)]$. Thus, (17) can be written as a linear equation:

$$q_i = (n-1)\, p_i + \nu \,. \tag{18}$$

The parameters n and ν can be determined using the least squares method:

$$\nu = \frac{\sum p_i \sum q_i\, p_i - \sum q_i \sum p_i^{\,2}}{\left(\sum p_i\right)^2 - N_1 \sum p_i^{\,2}} = \frac{\sum \ln \underline{h}_i \sum \ln \frac{\dot{z}_i}{\dot{\underline{h}}_i} \ln \underline{h}_i - \sum \ln \frac{\dot{z}_i}{\dot{\underline{h}}_i} \sum \left(\ln \underline{h}_i\right)^2}{\left(\sum \ln \underline{h}_i\right)^2 - N_1 \sum \left(\ln \underline{h}_i\right)^2}, \tag{19}$$

$$n = 1 + \frac{\sum p_i \sum q_i - N_1 \sum p_i\, q_i}{\left(\sum p_i\right)^2 - N_1 \sum p_i^{\,2}} = 1 + \frac{\sum \ln \underline{h}_i \sum \ln \frac{\dot{z}_i}{\dot{\underline{h}}_i} - N_1 \sum \ln \underline{h}_i \ln \frac{\dot{z}_i}{\dot{\underline{h}}_i}}{\left(\sum \ln \underline{h}_i\right)^2 - N_1 \sum \left(\ln \underline{h}_i\right)^2}, \tag{20}$$

where N_1 denotes the number of considered time points. For the same set of time points, using the calculated value and a discrete form of (2), the parameter A can be computed according to the formula:

$$A = \frac{1}{N_1} \sum z_i - \frac{1}{N_1} \sum \frac{e^{\nu}}{n} \underline{h}_i^{\,n} \,. \tag{21}$$

In order to identify all hysteresis parameters, determination of $\xi = \beta - \gamma$ is required. It can be done by calculation of the average value of parameter ξ in N_2 time points for which the relation $\dot{u}_j\, h_j < 0$ occurs:

$$\xi = \frac{1}{N_2} \sum \frac{z - A}{\underline{h}_j^{\,n}} \,. \tag{22}$$

Finally, the parameters β and γ can be calculated on the basis of v and ξ:

$$\beta = \frac{\xi}{2} - \frac{e^{\nu}}{2n}, \tag{23}$$

$$\gamma = -\frac{e^{\nu}}{2n} - \frac{\xi}{2} \,. \tag{24}$$

The main disadvantage of the estimation procedure described above is the necessity of using the second derivative, which significantly increases the effect of measurement errors. For this reason, in order to determine selected derivatives, the *continuum wavelet transform* (CWT) and the *translation-rotation transformation* (TRT) were used [19]. This method can significantly reduce the impact of noise and it enables to eliminate the boundary effect of traditional wavelet differentiation. Firstly, the TRT of function f is defined by:

$$f^{TRT}(t) = f(t) - at - b \,, \tag{25}$$

where:

$$a = \frac{f(t_{\max}) - f(t_{\min})}{t_{\max} - t_{\min}}, \quad b = f(t_{\min}) - a\, t_{\min} \,. \tag{26}$$

Afterwards, the derivative of function f can be calculated according to the formula:

$$\dot{f} = \frac{(f^{TRT})^{CWT}}{K s^{1.5} \Delta_t} + a \,, \tag{27}$$

Metrol. Meas. Syst., Vol. 24 (2017), No. 2, pp. 413–424.

where $(f^{TRT})^{CWT}$ is CWT of f^{TRT}, Δ_t is a time increment, s is the scale of CWT and K is a parameter depending on the used wavelet function ψ and it is defined as:

$$K = \int_{-\infty}^{\infty} \theta(t)dt \,. \tag{28}$$

A smoothing function θ is a time integral of the wavelet ψ with respect to time.

4. Determination of parameters of high-frequency piezoelectric actuators

In order to verify the described above method and its suitability for simulation of high-frequency PAs, experimental examinations were made. The object of research was a Noliac NAC2024 multilayer plate actuator (Fig. 2a) with dimensions 3 mm × 3 mm × 2 mm and an operating voltage in the range 0–200 V. A scheme of the experimental set-up is shown in Fig. 2b. The input voltage signal was generated by a Tektronix AFG 3022 function generator and enhanced by an EC Electronics PPA 2000 high-voltage amplifier. The signal was then transmitted to the actuator causing its displacement, which was recorded by the scanning head of Polytec PSV-3D-400-M laser vibrometer with a sampling frequency of 2.56 MHz.

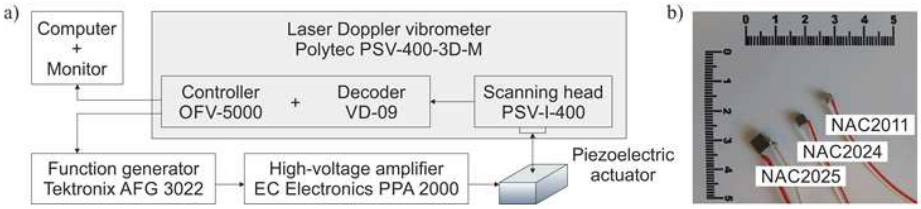

Fig. 2. Laboratory tests: a scheme of the experimental set-up (a); high-frequency PAs (centimetre scale) (b).

Determination of the mechanical parameters was made using a rectangular excitation with an amplitude of 7.8335 V and a period equal to 0.1 ms. Based on the measured input voltage signal, two parameters (T_1 = 1.8672 µs and a = 4.1954 MVs^{-1}) characterizing the excitation were identified. In the second step, based on the PA displacements in a period of 0–45 µs, a series of functions (g_0, g_1, and g_2) and the steady-state parameters K_0, K_1 and K_2 were defined (Fig. 3). It can be seen that the values of functions g_0 and g_1 rapidly converge to their limits, whereas for the function g_2 some oscillations are visible. It is related to the order of magnitude of this function and can result in inaccuracies in the identified steady-state value K_2. The mechanical parameters determined based on the above-mentioned values are summarized in Table 1.

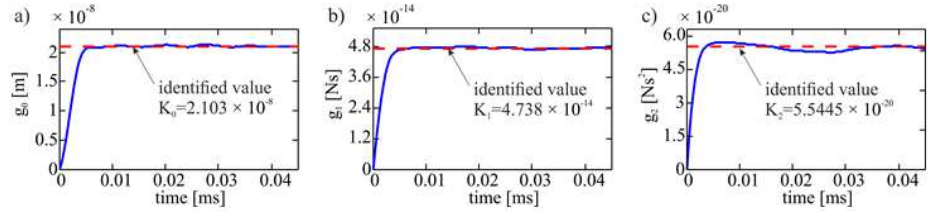

Fig. 3. The functions used for identification of the mechanical parameters of NAC2024 actuator: g_0 (a); b) g_1 (b); g_2 (c).

The procedure described in Section 3.2 can be applied to any type of excitation. However, the numerical tests showed that the best results can be obtained for a sinusoidal input voltage with a relatively large amplitude. The numerical tests also showed that in order to minimize the error associated with linearization, the identification procedure should be limited to a period in which the input voltage value is in a range of 25–75% of its amplitude. Therefore, to determine the hysteresis parameters for the actuator, a harmonic excitation with a frequency of 10 kHz and a magnitude of 9.738 V was used. The time variability of hysteresis component was determined on the basis of pre-determined mechanical parameters and the measured signal. In order to reduce the influence of noise, in determination of $\dot{h}$ and $\underline{\dot{h}}$ the CWT-TRT method was applied (Figs. 4b–4c). In numerical calculations the first order Gaussian wavelet (Fig. 4a) with a scale parameter $s = 4$ and the parameter $K = \sqrt[4]{2\pi}$ were used. It can be observed that using wavelet differentiation for $\underline{h}$ caused excessive smoothing in the jump area. However, this interval was not considered in the identification process. All other derivatives, including the PA velocity and acceleration time variations were determined using the central differential scheme.

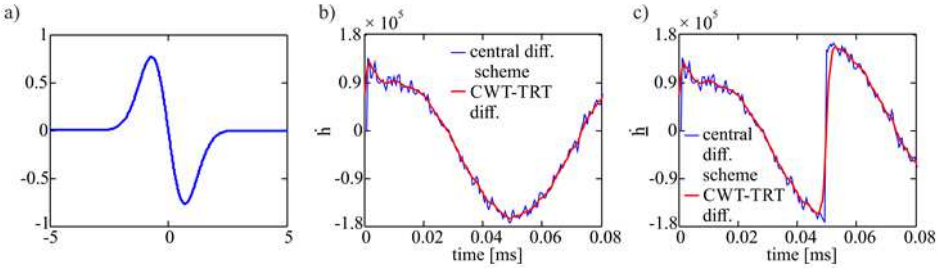

Fig. 4. Noise reduction for the hysteresis derivative: Gaussian wavelet of order 1 (a); comparison of finite difference and CWT-TRT differentiation of $\dot{h}$ (b); comparison of finite difference and CWT-TRT differentiation of $\underline{\dot{h}}$ (c).

The three-stage process of determining the hysteresis parameters is visualised in Fig. 5. In the first stage, the values of parameters v and n were determined using the least squares method and fitting the linear regression model to experimental data (Fig. 5a). In next stages, the values of A (Fig. 5b) and ξ (Fig. 5c) were determined by an averaging process. It can be noticed, that the experimentally determined data are scattered and no trend is clearly visible. This is a result of using the second derivative and occurring noise which influence can be limited using the CWT-TRT method by increasing the scale parameter s. However, the performed numerical tests using the Gaussian noise have shown that it does not affect correctness of the identification process. All identified parameters of (2) are listed in Table 1. Relatively low values of β and γ parameters indicate a small impact of non-linearity on the PA behaviour.

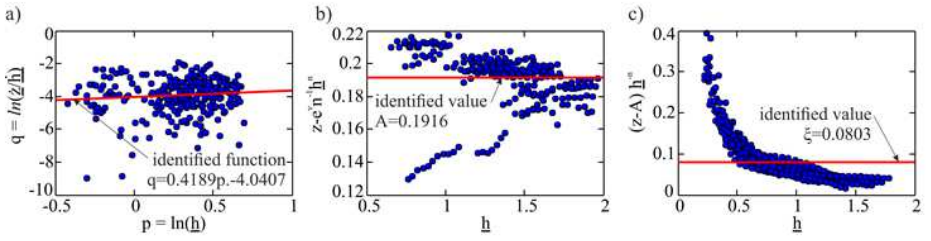

Fig. 5. Visualization of determining the hysteresis parameters: identification of v and n values using the least square method (a); identification of A value (b); identification of ξ value (c).

Metrol. Meas. Syst., Vol. 24 (2017), No. 2, pp. 413–424.

Table 1. A list of identified parameters of NAC2024 actuator for the modified symmetrical Bouc-Wen hysteresis model.

Parameter	m_0 [kg]	c_0 [kgs^{-1}]	k_0 [Nm^{-1}]	k_1 [V^{-1}]	A [–]	β [–]	γ [–]	n [–]
Identified value	3.419×10^{-4}	491.632	3.725×10^{8}	1	0.192	0.034	–0.0463	1.419

5. Experimental validation and accuracy analysis

In order to assess suitability of the model, additional tests comparing the experimental data with the results of numerical calculations were carried out. The simulations were performed using MATLAB® ordinary differential equation solver ode45 on the basis of the identified mechanical and hysteresis parameters and the experimentally measured input voltage signal. Selected results of the time variability of displacements and the hysteresis displacement-voltage loop are given in Fig. 6. It can be seen that the numerical and experimental results are in a good agreement in both initial and steady-state periods. The qualitative assessment of the model accuracy was made on the basis of global goodness-of-fit measures: the error *sum of squares* (SSE), the total *sum of squares* (SST), the *R*-squared (R^2), as well as a local correctness coefficient – the *maximum relative deviation* (MRD):

$$SSE = \sum_{i=1}^{N} (x_i - \hat{x}_i)^2 , \tag{29}$$

$$SST = \sum_{i=1}^{N} (x_i - \bar{x})^2 , \tag{30}$$

$$R^2 = 1 - \frac{SSE}{SST}, \tag{31}$$

$$MRD = \frac{\max\{| x_i - \hat{x}_i |\}}{\max\{x_i\}} \cdot 100\% , \tag{32}$$

where: x_i is the measured displacement; $\hat{x}_i$ is the numerically simulated displacement and $\bar{x}$ is the mean value of $\hat{x}_i$. The calculated values of specified error measures at different frequencies are summarized in Table 2.

Table 2. Statistical quantities characterizing the accuracy of predicted NAC2024 actuator displacements.

f [kHz]	10	20	40	60	80	100	120	140	160	180	200
SSE **[m]**	2,22 × 10^{-15}	2,52 × 10^{-14}	5,78 × 10^{-15}	2,27 × 10^{-15}	2,14 × 10^{-15}	2,46 × 10^{-15}	3,19 × 10^{-15}	3,28 × 10^{-15}	3,34 × 10^{-15}	5,2 × 10^{-15}	4,39 × 10^{-15}
SST **[m]**	1,971 × 10^{-12}	9,6 × 10^{-13}	4,32 × 10^{-13}	2,56 × 10^{-13}	1,71 × 10^{-13}	1,19 × 10^{-13}	8,69 × 10^{-14}	5,99 ×10^{-14}	4,33 × 10^{-14}	3,26 × 10^{-14}	1,94 × 10^{-14}
$\bar{x}$ **[m]**	–3,55× 10^{-11}	–2,33× 10^{-11}	–4,06× 10^{-11}	1,08 × 10^{-10}	–1,12× 10^{-10}	–6,0 × 10^{-12}	–2,25× 10^{-10}	–3,41× 10^{-10}	–1,12× 10^{-10}	–1,44× 10^{-10}	2,33 × 10^{-10}
R² [–]	0,999	0,974	0,987	0,991	0,987	0,979	0,963	0,945	0,923	0,840	0,774
MRD [%]	5,776	17,317	12,080	10,538	12,333	16,065	17,073	23,027	34,450	49,211	63,879

The results of the error analysis indicate effectiveness of the Bouc-Wen model and the proposed parameter identification method of simulating high-frequency PA motion. For all executed simulations in a range of 10–120 kHz, the correlation coefficient (R-square) between

the numerical and experimental results was greater than 0.95, which proves a good correspondence of the theoretical model results with the actual physical PA behaviour. The best fit was obtained for a frequency of 10 kHz, which was used for the model calibration. Fig. 6 shows that the maximum absolute error occurs in the maximum applied voltage area. An inaccuracy of the applied model significantly increases for frequencies of above 140 kHz. It is confirmed by a large value of MRD, at a level of 23% and more. An increase of the error value is caused by a relatively high uncertainty in determination of the mass, which influences high frequency oscillations. In addition, the available sampling frequency in experimental studies does not provide a sufficient number of sampling points for a period in a range above 100 kHz.

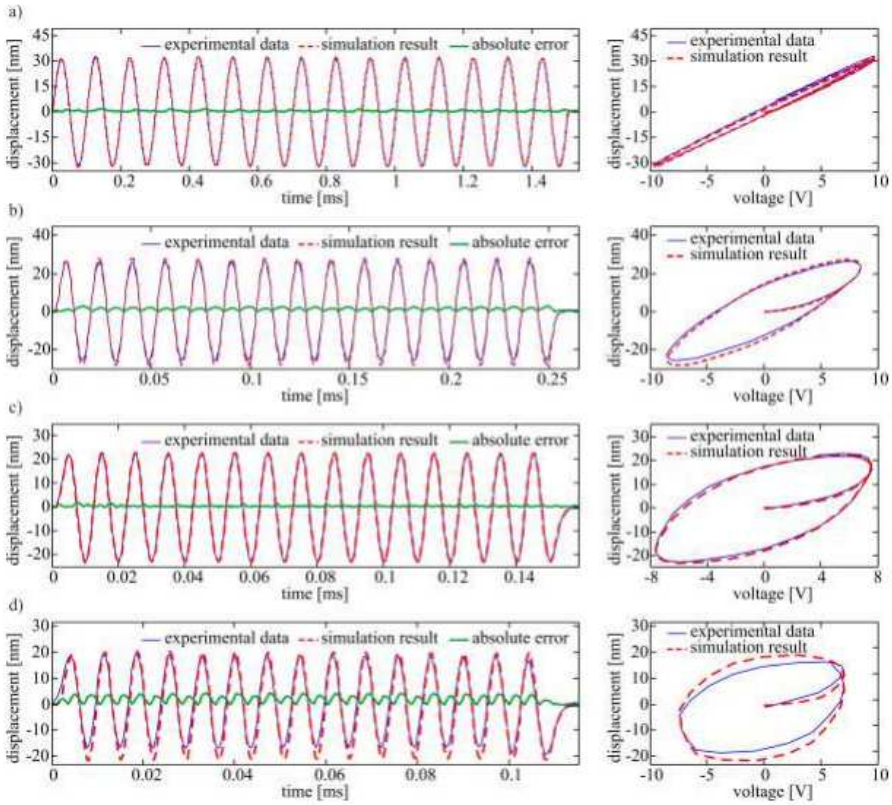

Fig. 6. Comparison of the numerical and experimental results for NAC2024 actuator – displacement versus time and displacement versus voltage in the initial stage, for a sinusoidal excitation with a frequency: 10 kHz (a); 60 kHz (b); 100 kHz (c); 140 kHz (d).

6. Conclusions

In the paper an improved two-step algorithm was proposed, dedicated to identifying the mechanical parameters of a modified, symmetrical Bouc-Wen model, adapted to characterize high-frequency piezoelectric actuators. An increase of accuracy in the first step of identification process, compared with algorithms used for low frequency PAs, was obtained by taking into account the initial variability of the excitation signal and assuming the ability of its approximation by a bilinear function. The hysteresis parameters of the Bouc-Wen model were determined in the second step, based on a single measured signal and using the CWT-TRT method for reducing an influence of noise.

Metrol. Meas. Syst., Vol. 24 (2017), No. 2, pp. 413–424.

The proposed algorithm was applied to modelling the mechanical behaviour of a high frequency PA. The Bouc-Wen model parameters were determined from the results of experimental tests using square and harmonic input voltage signals. Next, in order to validate the identification procedure, a comparative analysis was carried out. The tests aimed to compare the experimentally measured displacements of the tested PA and the numerical results obtained for the identified parameters of the Bouc-Wen model. The performed analyses have shown a good agreement between the experimental and numerical results in a range of 10–120 kHz. Above this range the model accuracy significantly decreases. It is caused primarily by inaccurate identification of the mass and by limitations of the assumed dynamic model. The proposed method of identification can be used for different types of hysteretic systems. The obtained results can be also useful in numerical modelling piezoelectric transducers for SHM systems.

References

[1] Sohrabi, M.A., Muliana, A. H. (2015). Nonlinear and time dependent behaviors of piezoelectric materials and structures. *Int. J. Mech. Sci.*, 94–95, 1–9.

[2] Gu, G., Zhu, L. (2011). Modeling of rate-dependent hysteresis in piezoelectric actuators using a family of ellipses. *Sensors Actuat. A-Phys.*, 165(2), 303–309.

[3] Wang, X., Pommier-Budinger, V., Reysset, A., Gourinat Y. (2014). Simultaneous compensation of hysteresis and creep in a single piezoelectric actuator by open-loop control for quasi-static space active optics applications. *Control Eng. Pract.*, 33, 48–62.

[4] Lin, C.-J., Lin, P.-T. (2012). Tracking control of a biaxial piezo-actuated positioning stage using generalized Duhem model. *Comput. Math. Appl.*, 64(5), 766–787.

[5] Liu X., Wang Y., Geng J., Chen Z. (2013). Modeling of hysteresis in piezoelectric actuator based on adaptive filter. *Sensors Actuat. A-Phys.*, 189, 420–428.

[6] Ghafarirad, H., Rezaei, S.M., Sarhan, A.A.D., Mardi, N.A., Zareinejad, M. (2014). A novel time dependent Prandtl-Ishlinskii model for sensorless hysteresis compensation in piezoelectric actuators. *IFAC Proceedings Volumes*, 47(3), 2703–2708.

[7] Zhu, W., Wang, D.H. (2012). Non-symmetrical Bouc-Wen model for piezoelectric ceramic actuators. *Sensors Actuat. A-Phys.*, 181, 51–60.

[8] Zhu, W., Rui, X.-T. (2016). Hysteresis modeling and displacement control of piezoelectric actuators with the frequency-dependent behavior using a generalized Bouc-Wen model. *Precis. Eng.*, 43, 299–307.

[9] Wang, D.H., Zhu, W. (2011). A phenomenological model for pre-stressed piezoelectric ceramic stack actuators. *Smart Mater. Struct.*, 20(3), 035018, (11 pp.).

[10] Wang, Z., Zhang, Z., Mao, J., Zhou, K. (2012). A Hammerstein-based model for rate-dependent hysteresis in piezoelectric actuator. *Proc. of the 2012 24th Chinese Control and Decision Conference*. Taiyuan, China, 1391–1396.

[11] Wang, G., Chen, G., Bai, F. (2015). High-speed and precision control of a piezoelectric positioner with hysteresis, resonance and disturbance compensation. *Microsyst. Technol.*, (11 pp).

[12] Xu, Q. (2013). Identification and compensation of piezoelectric hysteresis without modeling hysteresis inverse. *IEEE T. Ind. Electron.*, 60(60), 3927–3937.

[13] Bouc, R. (1967). Forced vibration of mechanical systems with hysteresis. *Proc. of the 4th Conference on Nonlinear Oscillation.*, Prague, Czechoslovakia, 315.

[14] Wen, Y.K. (1976). Method for random vibration of hysteretic systems. *J. Eng. Mech.-ASCE*, 102(2), 249–263.

[15] Low, T.S., Guo, W. (1995). Modeling of three-layer piezoelectric bimorph beam with hysteresis. *IEEE J. Microelectromech. Syst.*, 4(4), 230–237.

[16] Wang, Z., Mao, J. (2010). On PSO based Bouc-Wen modeling for piezoelectric actuator. *3rd International Conference on Intelligent Robotics and Applications.*, Shanghai, China, 125–134.

[17] Ha, J.L., Kung, Y.S., Fung, R.F., Hsien, S.C. (2006). A comparison of fitness functions for the identification of a piezoelectric hysteretic actuator based on the real-coded genetic algorithm. *Sensors Actuat. A-Phys.*, 132, 643–650.

[18] Wang, G., Chen, G., Bai, F. (2015). Modeling and identification of asymmetric Bouc-Wen hysteresis for piezoelectric actuator via a novel differential evolution algorithm. *Sensors Actuat. A-Phys.*, 235, 105–118.

[19] Luo J.W., Bai J., Shao J.H., (2006). Application of the wavelet transforms on axial strain calculation in ultrasound elastography. *Prog. Nat. Sci.*, 16(9), 942–947.